IEEE Access
Multidisciplinary | Rapid Review | Open Access Journal

Received September 4, 2020, accepted September 16, 2020, date of publication September 21, 2020,
date of current version October 1, 2020.

Digital Object Identifier 10.1109/ACCESS.2020.3025552

Performance Analysis of Rotary Magnetorheological Brake With Multiple Fluid Flow Channels

GUOLIANG HU, LIFAN WU, LINSEN LI, AND LIFAN YU
School of Mechatronics and Vehicle Engineering, East China Jiaotong University, Nanchang 330013, China
Corresponding author: Guoliang Hu (glhu@ecjtu.edu.cn)

This work was supported by the National Natural Science Foundation of China under Grant 51765016.

ABSTRACT In order to solve the problems of low magnetic field utilization rate and low volume-torque ratio of the traditional magnetorheological (MR) brake under a volume constraint, a rotary MR brake with multiple fluid flow channels was proposed. The magnetic flux was guided into the external axial fluid flow channel by inserting a non-magnetic ring in the middle of the magnetic conduction sleeves which could improve the magnetic circuit structure greatly, the working area where the MR brake producing rheological effect was increased, and the effective damping gaps were also increased from two sections to four sections. The working principle of rotary MR brake was expounded and torque mathematical model was also deduced. The electromagnetic field was modeled and the distribution of magnetic flux density in multiple fluid flow channels was analyzed using finite element method. The prototypes of initial and optimal design were fabricated by using the obtained optimal geometric parameters. An experimental test system was setup to investigate the dynamic performance of the proposed rotary MR brake. The experimental results show that the maximum braking torque and torque ratio of the optimal MR brake are increased by 13.5% and 2.3% compared with the initial MR brake at the applied current of 1.8 A, respectively. At the same time, the variation trend of experimental and simulation results is basically consistent, and the rotational speed has almost no effect on the torque performance, which is conducive to the application of MR brakes under different working conditions.

INDEX TERMS Rotary MR brake, multiple fluid flow channels, optimal design, braking torque.

I. INTRODUCTION

MR fluid, which is composed of magnetic particles and carrier fluid, is a kind of smart fluid [1]. It has a rapid dynamic response and controllable rheological properties, that is, under the action of an external magnetic field, magnetic particles can form a chain-like structure immediately, so that the fluid transforms into a semi-solid state. In the absence of the magnetic field, the fluid returns to the initial liquid state within milliseconds [2], [3]. Due to its rheological effect, the shear stress of the MR fluid can be continuously and reversely modified by the magnetic flux density [4], [5]. Based on these, MR fluid is widely applied in dampers [6]–[9], valves [10], [11], clutch and brake systems [12]–[14], and other industrial fields.

The associate editor coordinating the review of this manuscript and approving it for publication was Hamid Mohammad-Sedighi.

MR brake is a typical MR actuator, it has an excellent braking effect, simple structure, and low power consumption compared with traditional hydraulic brake [15]. Meanwhile, it can greatly simplify the complex structures and pipeline arrangement, reduce braking system manufacture and maintenance costs, and achieve coordinated control combined with electronic control system [16].

Over the last decades, scholars have designed a variety of MR brakes and got prominent achievements. However, under a volume constraint situation, most of the MR brakes have problems of insufficient braking torque and volume-torque ratio. It is difficult to realize the commercial application in high torque occasions, such as in the automobile braking system.

The current working mode of MR brake generally adopts the shear mode due to the friction between the rotor working surface and the MR fluid. From the perspective of brake structure design, there are mainly two ways to increase the

shear performance by increasing the magnetic flux density and damping gap length [17]–[19]. The magnetic flux density can be increased mainly by adding the number and size of excitation coils or optimizing the surface shape of damping gap. To a certain extent, adding the number or size of excitation coils on the single-coil MR brake can improve torque performance and reduce the response time, but the numbers of coils also lead to increasing the braking volume and power consumption [20]. Based on this, some scholars have studied the shape of the damping gap and the design of the magnetic circuit. Nam and Ahn [21] proposed a novel brake incorporation a rotary disk with a waveform boundary that generates a resistance force based on the effect of a material deformation process. The resistance forces and the braking torque generated by this crush action are stronger than those produced by strain action. Senkal and Gurocak [22] presented a MR brake with a serpentine flux path. Magnetically conductive and non-conductive elements were stacked to weave the magnetic flux through the rotor and the outer shell of the MR brake. The results show that the MR brake is compact and powerful. Qin *et al.* [23] developed a hybrid actuator with hollowed multi-drum MR brake and DC micromotor, and the micromotor was placed inside the MR brake to obtain a compact structure. Results proved that the hybrid actuator has great torque than the single MR brake. Nguyen and Shiao [24] designed a multi-pole MR brake, which adopts multiple excitation coils evenly arranged to form multiple magnetic poles, further enhance the braking torque of the drum brake. Wang and Bi [25] designed a MR brake with compression shear mode. Under the conditions of high pressure and small damping gap, the braking torque was significantly improved.

The above innovative design methods of damping gap surface and magnetic flux path can improve braking torque to a certain extent. But the complex gap surface and the optimized yoke are more difficult to fabricate, which increases the manufacturing cost and the number of moving parts. On the basis of structural design, some researchers adopt optimization algorithm to minimize the structure of MR brake and improve its performances as well. Assadsangabi *et al.* [26] improved the disc-type MR brake by using genetic algorithm. The effective area was added to the optimized rear brake, thus increasing braking torque. Nguyen and Choi [27] adopted the Golden section algorithm to optimize the design of the MR brake geometric dimensions under the consideration of braking torque and zero-field friction heat, so as to have a larger braking torque and a smaller mass. Later on, Nguyen and Choi [28] optimized the common MR brake types under a constrained volume, including disc-type, drum-type, and hybrid-type. The method of combining FEM analysis and optimization tools was used to determine the optimal value of the significant dimensions that affect braking torque. Qin *et al.* [29] adopted the multi-objective genetic algorithm to optimize the design of multi-drum brake and determined the optimal number of brake drums under different flow gaps. Le-Duc *et al.* [30] used multi-objective optimization combined with finite element analysis to optimize the MR brake. The optimization focuses on maximizing the brake torque under the premise of reducing the weight requirements. Mousavi and Sayyaadi [31] optimized a hybrid MR brake for prosthesis knee joint by using particle swarm optimization, taking torque, energy consumption, and torque density as objective functions. Topcu *et al.* [32] introduced a modified particle swarm optimization algorithm to solve the multi-physics engineering optimization problem for the rotary MR brake. The optimized MR brake has a smaller volume and greater braking torque. The above optimization design improves braking performance to some extent, but the optimization objective does not consider some important performance indexes, such as the torque ratio. The optimization process is mostly based on the MR brake with traditional structure, and the brake torque is still small, which is more suitable for artificial limbs and tactile devices. In order to further broaden the application scope of the MR brake and completely achieve its application in the large braking torque field, it is necessary to design a MR brake with large torque and wide controllable range.

In this paper, a rotary MR brake with multiple fluid flow channels for automobile is designed and developed. It is different from the traditional drum-type MR brake with a single fluid flow channel, the MR fluid flow channels are divided into inside layer and outside layer, and the MR brake obtains a larger effective working area with a compact volume. Based on finite element simulation, the braking torque and torque ratio of the MR brake are improved by optimizing significant dimensions combined with first-order optimization tools. Finally, MR brake prototypes of initial and optimal design were fabricated, respectively. The braking torque is tested, and performance improvement of the optimal MR brake is also discussed.

II. STRUCTURAL DESIGN AND MAGNETIC CIRCUIT ANALYSIS OF THE PROPOSED MR BRAKE

A. STRUCTURAL DESIGN AND PRINCIPLE OF THE PROPOSED MR BRAKE

The arrangement of the fluid flow channels of the MR brake is an important factor that affects braking performance. The best rheological effect and the largest shear stress can be obtained if the magnetic flux lines pass through vertically to the fluid flow channels. On this basis, FIGURE 1 presents the developed MR brake with multiple fluid flow channels. The MR brake is mainly consisted of rotating sleeve, magnetic core, rotating shaft, end covers, cylinder tube, and excitation coil. Among them, rotating sleeve is composed of a non-magnetic ring, left and right magnetic conduction sleeve, and magnetic conduction sleeves are respectively connected with non-magnetic ring through threads, which are cured and locked by thread glue. Rotating sleeve and rotating shaft are connected by bolts, and rotating shaft drives the rotation. Except that non-magnetic ring and end covers are made of stainless steel, the other parts are all made of low carbon steel magnetic conduction material.

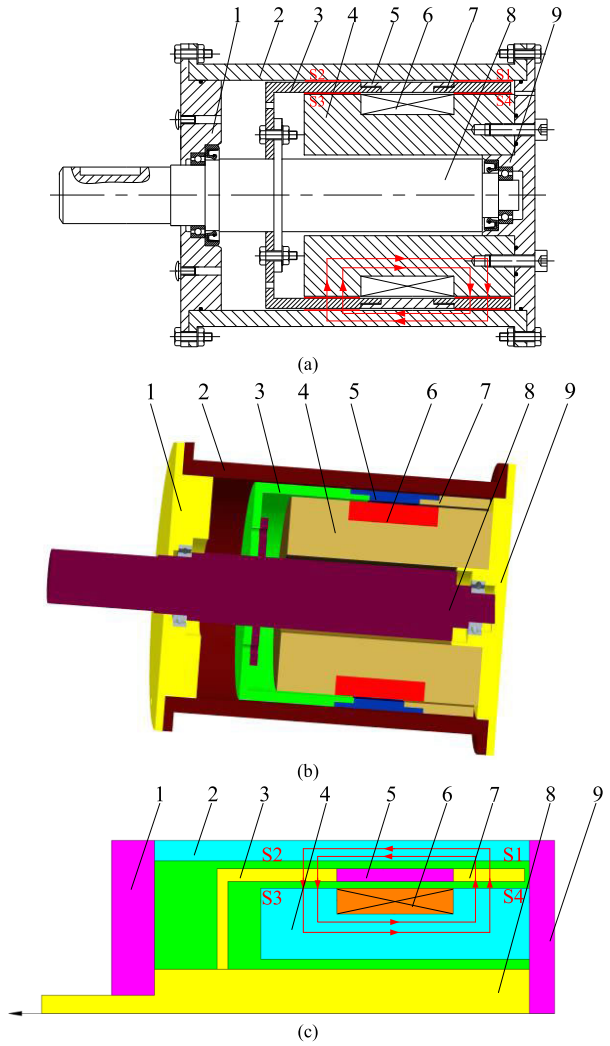

FIGURE 1. Structure diagram of MR brake with multiple fluid flow channels: (a)Structural schematic, (b) Three-dimensional sectional view, and (c) Magnetic circuit diagram. (1) Left end cover (2) Cylinder tube (3) Left magnetic conduction sleeve (4) Magnetic core (5) Non-magnetic ring (6) Excitation coil (7) Right magnetic conduction sleeve (8) Rotating shaft (9) Right end cover.

As shown in FIGURE 1, the external axial fluid flow channel is enclosed by cylinder tube and rotating sleeve. Also, the inner axial fluid flow channel is enclosed by magnetic core and rotating sleeve. Inserting a non-magnetic ring in the middle of rotating sleeve can reverse the magnetic flux line to the unused external axial fluid flow channel, thereby guiding the magnetic flux line to vertically pass through the four effective damping gaps. In the external axial fluid flow channel, there are two effective damping gaps S1 and S2. In the inner axial fluid flow channel, there are two effective damping gaps S3 and S4. This design can effectively increase the damping gap lengths of rheological effect and improve braking torque without increasing the number of moving parts. Considering rheological properties of MR fluid, the damping gap size is set as 1.0 mm to prevent the channel from blocking. The external diameter of the MR brake is 120 mm, and the total axial length is 173 mm.

Owing to the principle of electromagnetic induction, a magnetic field is generated at the fluid flow paths under the applied current. Firstly, magnetic flux line passes through the magnetic core, the effective damping gap S3, rotating sleeve, and the effective damping gap S2, and reaches cylinder tube, then vertically passes through the effective damping gap S1, rotating sleeve, and passes through the effective damping gap S4, finally back to magnetic core. As a result, a closed loop is formed. When the excitation coil is energized to generate a magnetic field, MR fluid changes from a fluid to a semi-solid state. Due to the rheological properties, the shear yield stress increases, this in turn generates a larger braking torque to achieve braking effect. Changing the applied current to control the shear yield stress can attain stepless adjustment of braking torque.

B. MAGNETIC CIRCUIT OF THE PROPOSED MR BRAKE

FIGURE. 2 shows the simplified magnetic circuit of MR brake with multiple fluid flow channels. The magnetic flux lines pass through magnetic core, rotating sleeve, cylinder tube, and four section gaps.

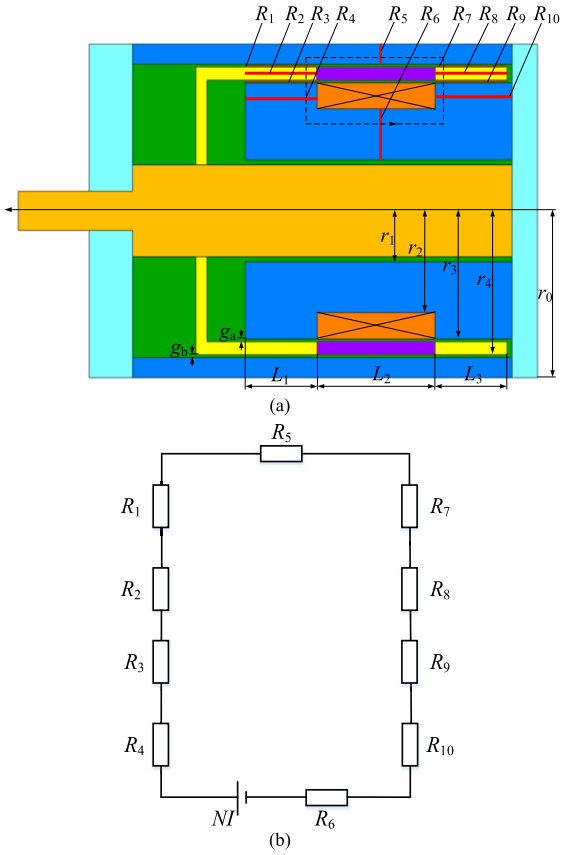

FIGURE 2. Magnetic circuit of MR brake: (a) The simplified Magnetic, and (b) Equivalent magnetic circuit model.

Assuming that magnetic flux lines are uniformly distributed and magnetic flux leakage is ignored, the magnetic

flux in the loop is defined as:

$$\Phi_r = \Phi_l = \Phi_{steel} = \Phi \tag{1}$$

where Φ is the total magnetic flux, Φ_l is the magnetic flux through the sections S1 and S4, Φ_r is the magnetic flux through the sections S2 and S3, and Φ_{steel} is the magnetic flux of magnetically conductive parts such as rotating sleeve, cylinder, and magnetic core.

Applying Kirchhoff's law to analyze the magnetic circuit, the magnetomotive force can be expressed as:

$$N_c I = \oint_c H \mathrm{d}l = \sum_{i=1}^{10} H_i l_i \tag{2}$$

where N_c is the number of turns of excitation coil, I is the applied current, H_i is the magnetic field intensity of the ith effective part of the magnetic circuit, and l_i is the effective length of the ith path in the magnetic circuit.

The total magnetic flux generated by the excitation coil can be denoted as:

$$\Phi = \oint_c B \mathrm{d}S = B_i S_i \tag{3}$$

where B_i is the magnetic flux density of the i th effective part in the magnetic circuit, and S_i is the cross-sectional area of the ith effective part.

The relationship between the magnetic flux density B_i and the magnetic field intensity H_i of the ith effective part can be expressed as:

$$B_i = \mu_0 \mu_i H_i \tag{4}$$

where μ_0 is permeability of vacuum, and μ_i is the relative permeability of the material.

The magnetic reluctance of the effective part can be calculated as:

$$R_i = \frac{l_i}{\mu_0 \mu_i S_i} \tag{5}$$

The magnetic reluctance of the external axial damping gap can be expressed as:

$$R_1 = R_7 = \frac{g_b^2}{\pi \left[(r_4 + g_b)^2 - r_4^2\right] L_1 \mu_0 \mu_2} \tag{6}$$

The magnetic reluctance of the effective part of the rotating sleeve can be regarded as:

$$R_2 = R_8 = \frac{(r_4 - r_3 - g_a)^2}{\pi \left[r_4^2 - (g_a + r_3)^2\right] L_1 \mu_0 \mu_1} \tag{7}$$

The magnetic reluctance of the internal axial damping gap can be denoted as:

$$R_3 = R_9 = \frac{g_a^2}{\pi \left[(r_3 + g_a)^2 - r_3^2\right] L_1 \mu_0 \mu_2} \tag{8}$$

The magnetic reluctance of the magnetic core flanks is:

$$R_4 = R_{10} = \frac{(r_3 - r_2)^2}{\pi (r_3^2 - r_2^2) L_1 \mu_0 \mu_1} \tag{9}$$

The magnetic reluctance of the cylinder can be expressed as:

$$R_5 = \frac{L_1 + L_2}{\pi \left[r_0^2 - (r_4^2 + g_b)^2\right] \mu_0 \mu_1} \tag{10}$$

The magnetic reluctance of the magnetic core central section can be expressed as:

$$R_6 = \frac{L_1 + L_2}{\pi (r_2^2 - r_1^2) \mu_0 \mu_1} \tag{11}$$

As a result, the total magnetic reluctance can be expressed as:

$$R_m = 2 (R_1 + R_2 + R_3 + R_4) + R_5 + R_6 \tag{12}$$

According to Eqs. (2)-(4), the following equation can be obtained:

$$N_c I = \sum_{i=1}^{10} \frac{B_i}{\mu_0 \mu_i} l_i = \sum_{i=1}^{10} \frac{l_i}{\mu_0 \mu_i S_i} \Phi = \sum_{i=1}^{10} R_i \Phi \tag{13}$$

Therefore, the magnetic flux density of each effective part can be calculated as:

$$B_i = \frac{\Phi}{S_i} = \frac{N_c I}{S_i \sum_{i=1}^{10} R_i} \tag{14}$$

The magnetic flux density of the external axial damping gaps can be calculated as:

$$B_1 = B_2 = \frac{\Phi}{S_1} = \frac{N_c I}{S_1 \sum_{i=1}^{10} R_i} \tag{15}$$

The magnetic flux density of the inner axial damping gaps can be calculated as:

$$B_3 = B_4 = \frac{\Phi}{S_3} = \frac{N_c I}{S_3 \sum_{i=1}^{10} R_i} \tag{16}$$

C. MATHEMATICAL MODEL OF BRAKING TORQUE OF THE PROPOSED MR BRAKE

At present, the Bingham model and Herschel-Bulkley model are applied to describe the rheological properties of MR fluid most widely, and the difference is that the latter considers the effect of shear thinning and shear thickening on the shear stress. Because the Bingham model has few unknown parameters and the results can accurately describe the rheological properties of the MR fluid at moderate shear rates, it was selected as the basis for the torque model in this paper. The stress-strain relationship of the Bingham model is as follows:

$$\tau = \tau(B) \mathrm{sgn}(\dot{\gamma}) + \eta \dot{\gamma} \tag{17}$$

where τ is MR fluid shear stress, τ(B) is yield stress varying with magnetic flux density, η is viscosity of MR fluid without magnetic field, and $\dot{\gamma}$ is shear strain rate.

When the rotating shaft drives the rotating sleeve to rotate, the flow direction of MR fluid is shown in FIGURE. 3.

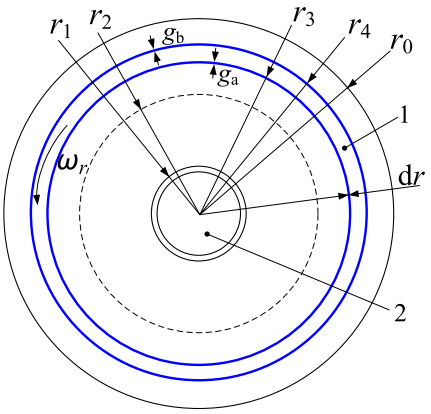

FIGURE 3. Circumferential flow diagram of MR fluid. (1) Rotating sleeve (2) Rotating shaft.

The braking torque of the proposed MR brake can be calculated as:

$$T = 2\pi r^2 L\tau \tag{18}$$

where L is damping gap length, and r is annular damping gap radius.

The shear strain rate of MR fluid in the damping gap can be expressed as:

$$\dot{\tau} = r\frac{\mathrm{d}\omega_r}{\mathrm{d}_r} \tag{19}$$

where ω_r is rotational speed of MR fluid at radius of r.

Assuming that MR fluid is evenly distributed in different damping gap, the differential of the rotation speed can be obtained from Eqs. (17)-(19), which is as follows:

$$\mathrm{d}\omega_r = \frac{1}{\eta}\left(\frac{T}{2\pi Lr^3} - \frac{\tau(B)}{r}\right)\mathrm{d}r \tag{20}$$

Under the linear distribution of MR fluid's radial velocity, the boundary conditions of the inner axial damping gap are:

$$r = \begin{cases} r_3 & (\omega_r = 0) \\ r_3 + g_a & (\omega_r = \omega) \end{cases} \tag{21}$$

The boundary conditions of the external axial damping gap are:

$$r = \begin{cases} r_4 + g_b & (\omega_r = 0) \\ r_4 & (\omega_r = \omega) \end{cases} \tag{22}$$

According to Eqs. (20) and (21), the braking torque T_1 of the inner axial damping gap is:

$$T_1 = \frac{4\pi L\tau(B)r_3^2(r_3+g_a)^2\ln((r_3+g_a)/r_3)}{(r_3+g_a)^2 - r_3^2} + \frac{4\pi\eta Lr_3^2(r_3+g_a)^2\omega}{(r_3+g_a)^2 - r_3^2} \tag{23}$$

According to Eqs. (20) and (22), the braking torque T_2 of the external axial damping gap is:

$$T_2 = \frac{4\pi L\tau(B)r_3^2(r_3+g_a)^2\ln((r_3+g_a)/r_3)}{(r_3+g_a)^2 - r_3^2} + \frac{4\pi\eta Lr_3^2(r_3+g_a)^2\omega}{(r_3+g_a)^2 - r_3^2} \tag{24}$$

The size of the internal and external damping gap is:

$$h = g_a = g_b \tag{25}$$

Assume that the size of the damping gap is much less than the radius of the rotating sleeve ($h/r_4 \ll 1$). Via Eqs. (23) and (25), the following equation can be obtained:

$$T_1 = 2\pi L\tau(B)r_3^2 + \frac{2\pi\eta L\omega r_3^3}{h} \tag{26}$$

Via Eqs. (24) and (25), the following equation can be obtained:

$$T_2 = 2\pi L\tau(B)(r_4+g_b)^2 + \frac{2\pi\eta L\omega(r_4+g_b)^3}{h}\ldots \tag{27}$$

It can be seen from Eqs. (26) and (27) that the torque generated by MR brake is mainly composed of two parts, the first one is the controllable torque generated from rheological effect, and the latter one is the torque generated from viscosity of MR fluid. Therefore, the total braking torque can be expressed as:

$$T = T_B + T_\eta \tag{28}$$

Here, T_B and T_η can be written as:

$$T_B = 2\pi L\tau(B)r_3^2 + 2\pi Lr(B)(r_4+g_b)^2 \tag{29}$$

$$T_\eta = \frac{2\pi\eta L\omega r_3^3}{h} + \frac{2\pi\eta L\omega(r_4+g_b)^3}{h} \tag{30}$$

III. MAGNETIC FIELD SIMULATION ANALYSIS

The MR fluid is in a long-term shear state inside the MR brake, and the ferromagnetic particles in the carrier fluid will be broken into smaller fragments, leading to the change of the overall rheological property. Therefore, the durability of the MR fluid is an important index to prolong the service life of the brake. The MR fluid used in the MR brake is MRF-J01T manufactured by Chongqing Materials Research Institute in China. The relevant performance indexes of the MRF-J01T are listed in TABLE 1. This type of MR fluid has good rheological properties and durability, which can well meet the requirements of the experimental test. Ordinary least squares was used to fit the τ-B curve of the MR fluid with cubic polynomial, and the relation between the shear yield stress and magnetic flux density at the damping gap was obtained as follows:

$$\tau(B) = a_3B^3 + a_2B^2 + a_1B + a_0 \tag{31}$$

where a_3, a_2, a_1, a_0 respectively expressed as polynomial coefficients, here, $a_3 = -984.27$ kPa/T^3, $a_2 = 865.39$ kPa/T^2, $a_1 = -48.46$ kPa/T, and $a_0 = 0.02$ kPa.

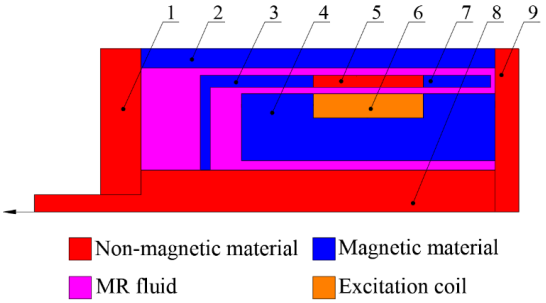

FIGURE 4. Entity model of the proposed MR brake. (1) Left end cover (2) Cylinder tube (3) Left magnetic conduction sleeve (4) Magnetic core (5) Non-magnetic ring (6) Excitation coil (7) Right magnetic conduction sleeve (8) Rotating shaft (9) Right end cover.

TABLE 1. Properties of MRF-J01T.

Property	Values
Density (ρ/g·cm^{-3})	2.65
Viscosity at 20 ℃(η/ Pa·s)	0.8
Shear stress at 0.5T (τ_y/ kPa)	>50
Magnetic properties (M_s/ KA·m^{-1})	379.64
operating temperature (T/℃)	-40~130

A two-dimensional finite element model was established by using ANSYS finite element simulation software without considering the magnetic flux leakage phenomenon at the magnetic field boundary, as shown in FIGURE. 4. In view of that, the cross-sections of the MR brake is regular axisymmetric, half of the cross-section is selected as the simulation object without affecting the simulation accuracy. The element type is defined as the quadrilateral PLANE13 element with 4 nodes, the number of elements used is 77759, and element degrees of freedom is 1. The model is meshed by SmartSize and the meshing level is 1. In order to get a more accurate solution, the damping gaps are meshed again. From the perspective of modeling technology and magnetic circuit design, the hysteresis of magnetic material has a great impact on the controller's tracking torque performance. Magnetic core, magnetic conduction sleeves, and the cylinder tube are all made of steel No. 10 with excellent magnetization and hysteresis performance.

FIGURE 5 shows the finite element analysis of MR brake at the applied current of 1.0 A. As can be seen from FIGURE 5(a), the magnetic flux lines form a closed loop through the cylinder tube by setting a non-magnetic ring in the middle of rotating sleeve. The external axial flow channel between rotating sleeve and cylinder tube is fully utilized to form four effective damping gaps, which improve

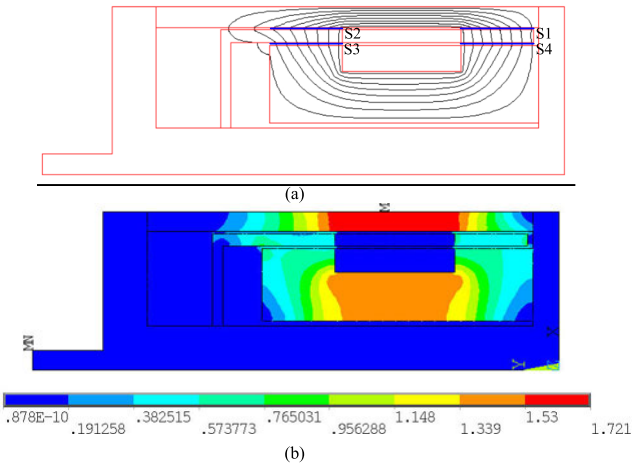

FIGURE 5. Finite element analysis of the MR brake: (a) Distribution of magnetic flux lines, and (b) Contour of magnetic flux density.

the utilization rate of magnetic field. In addition, almost all magnetic flux lines pass vertically through damping gap S2 and S3, but there is a part of magnetic flux leakage on the left of damping gap S2. This is because the left magnetic conduction sleeve is made of steel No. 10, which has better magnetic permeability than MR fluid, leading to a small part of magnetic flux lines form a closed loop on the left of damping gap S2.

Figure 5(b) shows the contour of the distribution of magnetic density. Observing figure 5(b), the cross-sectional area of the cylinder body is small and the magnetic flux density is the largest. Near the excitation coil area, the closer to the excitation coil, the greater the magnetic flux density. Hence, the magnetic flux density at both ends of the flow channels also varies with the path distance from the excitation coil.

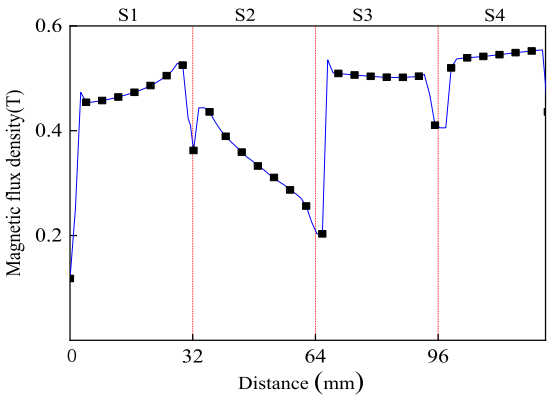

FIGURE 6. Magnetic flux density along the defined fluid flow channels.

FIGURE 6 shows the magnetic flux density variation of damping gap S1, S2, S3, and S4 along the path when the current is 1.0 A. It can be observed that the magnetic flux density of damping gap S1 increases with the path distance. This is because there is a radial fluid flow channel on the right of damping gap S1, and the magnetic flux lines in the

magnetic conductivity area around the right of damping gap S1 cannot be concentrated, resulting in the decrease of the total magnetic flux. The magnetic flux density of damping gap S2 decreases with the increase of path distance, which confirms that there is partial magnetic flux leakage on the left of damping gap S2 in the magnetic flux line analysis above. The magnetic flux density distribution of damping gap S3 and S4 is more stable than that of S2 and S1. The magnetic flux density is smaller at both ends and concentrated in the middle section of the gap, with great magnetic permeability.

IV. OPTIMIZATION OF THE PROPOSED MR BRAKE

A. MECHANICAL PERFORMANCE OPTIMIZATION

On the basis of determining structure, reasonable optimization design of the magnetic circuit can make the actual performance of MR brake better. On the premise of meeting the design size of the system, the optimization function of ANSYS software was utilized to optimize the size of the MR brake. By using the first order optimization tool with high sensitivity and accuracy to design variables, the linear weighted grouping method was adopted to construct the objective function to achieve the multi-objective optimization. The optimization process is shown in FIGURE 7.

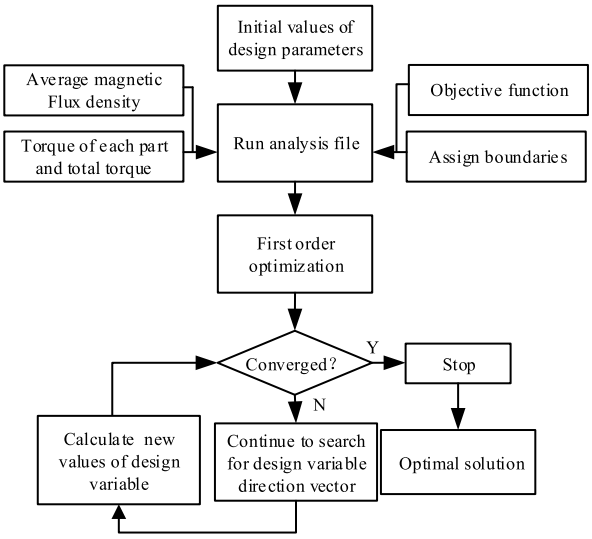

FIGURE 7. Flowchart of optimization design.

A good MR brake should have high braking torque and the torque ratio, where the torque ratio is defined as:

$$K = T_B/T_\eta \tag{32}$$

where T_B is magnetic induced torque, and T_η is viscous induced torque.

Considering the impact of the above two indexes on the comprehensive performance requirement of the MR brake, the corresponding indicator weight coefficients are set up to construct the objective function, which is defined as:

$$f = \frac{T}{T^*} \times \lambda_1 + \frac{K}{K^*} \times \lambda_2 \tag{33}$$

where T is braking torque of initial design, T^* is braking torque of optimal design, K is the torque ratio of initial design, K^* is the torque ratio of optimal design, λ_1 is braking torque weight coefficient, and λ_2 is the torque ratio weight coefficient.

The performance of the MR brake was optimized, and the optimization design variables were selected, as shown in TABLE 2. Considering the low magnetic flux density of path S2, the state variable was set as the average magnetic flux density $B \geq 0.4$ T for each path, and the number of iterations was set as 20.

TABLE 2. Optimized design variables of MR brake.

Design variables	Upper limit (mm)	Lower limit (mm)
Cylinder thickness (*WE*)	10	5
Rotating sleeve thickness (*WD*)	8	3
Non-magnetic ring length (*TC*)	50	40
Magnetic core thickness (*WC*)	35	20
Left radial gap width (*TD*)	20	5
Right radial gap thickness (*GAP*)	4	1

In order to make the MR brake more suitable for medium and high speed braking occasions for automobile, larger braking torque is required, and the requirement for torque ratio is lower. Therefore, two sets of similar weight coefficients ($\lambda_1 = 0.7$ and $\lambda_2 = 0.3$, $\lambda_1 = 0.8$ and $\lambda_2 = 0.2$) were selected according to the requirements of actual working occasions to obtain the optimization results. FIGURE 8 shows the variation of relevant parameter with the optimization iterations when the objective function weight coefficient is $\lambda_1 = 0.7$ and $\lambda_2 = 0.3$, and the applied current is 1 A. It can be seen that the objective function gets the minimum value at the fifth loop iteration, and the final optimization result is obtained, in which the maximum average magnetic flux density is 0.53 T, the optimal braking torque and torque ratio are 85.33 N·m and 34.38, respectively.

The optimization results are listed in TABLE 3. The results demonstrate that the torque performance of the brake can be significantly improved by selecting the optimal geometrical parameters. At the same time, comprehensive consideration of the braking torque and torque ratio can avoid higher viscous induced torque.

Two different optimization results are obtained for the different values of the two index weight coefficients in the objective function:

(1) When the weight coefficient is $\lambda_1 = 0.7$ and $\lambda_2 = 0.3$, braking torque increases from 63.39 N·m to 85.33 N·m, increasing by 34.6%; the torque ratio increases from 33.3 to 34.38, with an increase of 3.2%.

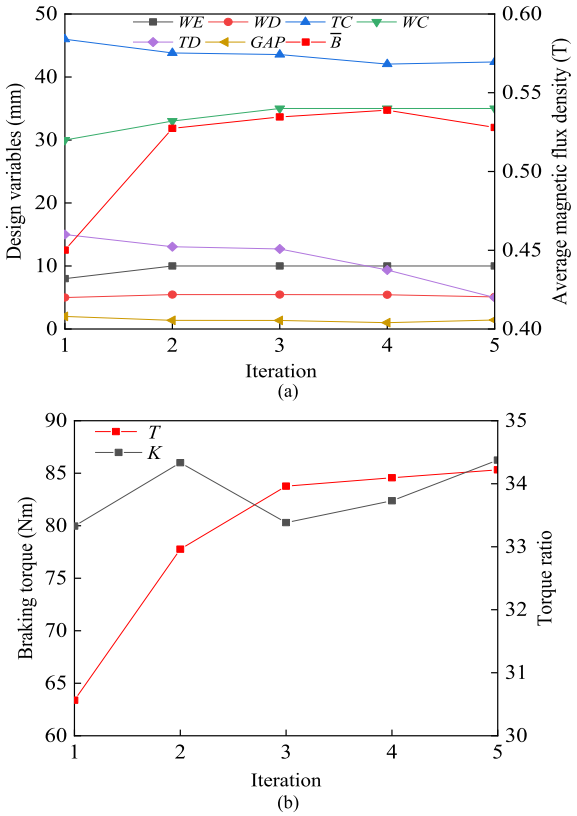

FIGURE 8. Multi-objective optimization iteration results of MR brake: (a) Design variables and average magnetic flux density, and (b) Braking torque and torque ratio.

(2) When the weight coefficient is λ_1 =0.8 and λ_2 = 0.2, braking torque increases from 63.39 N·m to 88.10 N·m, increasing by 38.98%; the torque ratio increases from 33.33 to 33.64, with an increase of 0.09%.

From the optimization results, it can be concluded that the proposed MR brake obtains a great torque performance improvement when the weight coefficient is λ_1 = 0.7 and λ_2 = 0.3. At the same time, the torque ratio also has a certain increase. Therefore, this group of optimization data is selected for analysis of optimization simulation results.

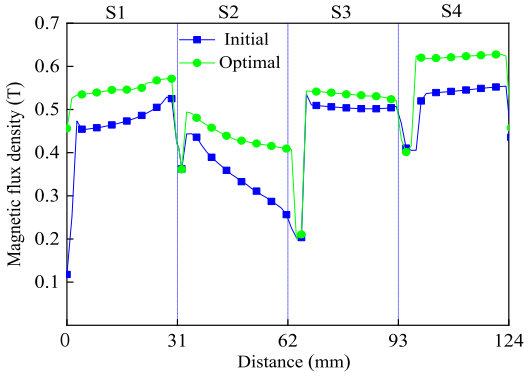

FIGURE 9. Magnetic flux density along the fluid flow paths.

TABLE 3. Results of initial design and optimal design.

Parameters	Initial	Optimal (λ_1, λ_2)	
		(0.7,0.3)	(0.8,0.2)
Objective function *(f)*	1	0.81088	0.7738
Braking torque *(T*/Nm*)*	63.39	85.33	88.10
The torque ratio *(K)*	33.33	34.38	33.64
Average magnetic flux density of S1 (B_1/T)	0.457	0.540	0.554
Average magnetic flux density of S2 (B_2/T)	0.330	0.433	0.427
Average magnetic flux density of S3 (B_3/T)	0.484	0.522	0.534
Average magnetic flux density of S4 (B_4/T)	0.529	0.617	0.654
Cylinder thickness (*WE*/mm)	8	10	10
Rotating sleeve thickness (*WD*/mm)	5	5.1	7
Non-magnetic ring length (*TC*/mm)	46	42.4	40
Magnetic core thickness (*WC*/mm)	30	35	35
Left radial gap width (*TD*/mm)	15	5	5
Right radial gap thickness (*GAP*/mm)	2	1.43	1.333

B. OPTIMIZATION RESULT ANALYSIS

FIGURE 9 shows the variation of magnetic flux density distribution of the initial MR brake and optimal MR brake at the applied current of 1 A. It can be seen that the magnetic flux density distribution value in the optimal MR brake damping gap has a large increase, and the magnetic flux density of path S1 and path S2 also has a great improvement with the increasing or decreasing trend, the distribution of magnetic flux density is more uniform, which indicates that the average magnetic flux density in each path has been improved to a certain extent compared with that initial design, and the MR brake performance has been improved after optimization. The increase in the average magnetic flux density of damping gap is mainly due to the reduction of the numerical optimization of the left radial gap width. At this time, the magnetic reluctance in the MR brake magnetic circuit decreases, the total magnetic flux increases, and the magnetic flux lines are more concentrated and evenly distributed in the magnetic circuit. The magnetic flux lines passing vertically through damping gap are also denser, so the magnetic field distribution in the path S2 is better improved.

Based on the magnetic flux density at path S2 in FIGURE 9, the corresponding shear yield stress curve in FIGURE 10 is obtained. It can be seen that the variation trend

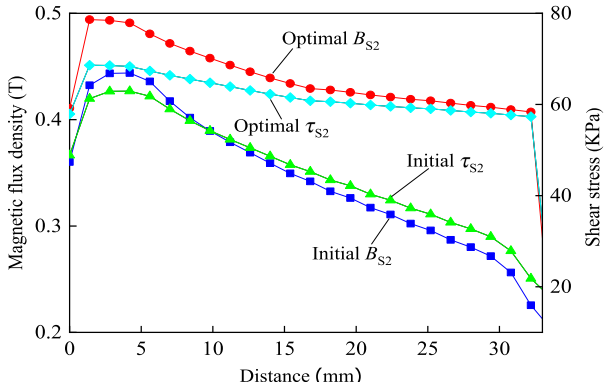

FIGURE 10. Variation of magnetic flux density and shear stress along path S2.

of the yield stress along the path at the damping gap of S2 is similar to that of the magnetic flux density. The calculation shows that the optimized average shear yield stress can reach 60.2 kPa, which is 35.1% more than the 44.56 kPa of initial design. It is further confirmed that magnetic circuit design effect of the optimal MR brake is better.

FIGURE 11 shows the variation curve of the average magnetic flux density in the damping gap of the optimal MR brake. It can be seen that although the average magnetic flux density in each damping gap is different, it all increases with the increase of applied current. This is because the magnetomotive force in the magnetic circuit also increases after the increase of current, so the average magnetic flux density increases. When the current is 1.0 A, the average magnetic flux density in the damping gap can reach 0.528 T, which can meet the design requirements.

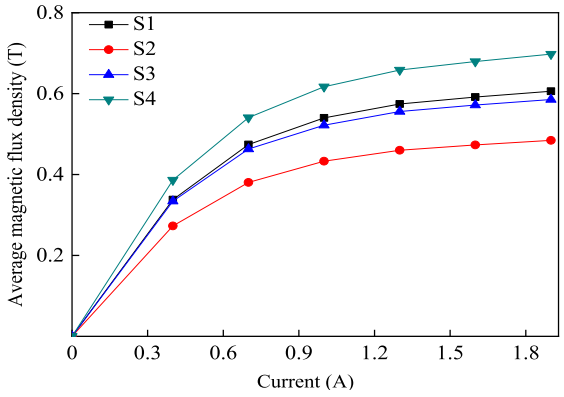

FIGURE 11. Variation of the optimized average magnetic flux density.

FIGURE 12 shows the optimized braking torque varies with the rotational speed when the brake is input with different current. Observing FIGURE 12, the speed has little effect on braking torque at a certain current. It is because the viscous induced torque has little influence on the overall braking torque. Therefore, braking torque of the MR brake is approximately equal at the same current and different rotational speeds, so the average value of braking torque at

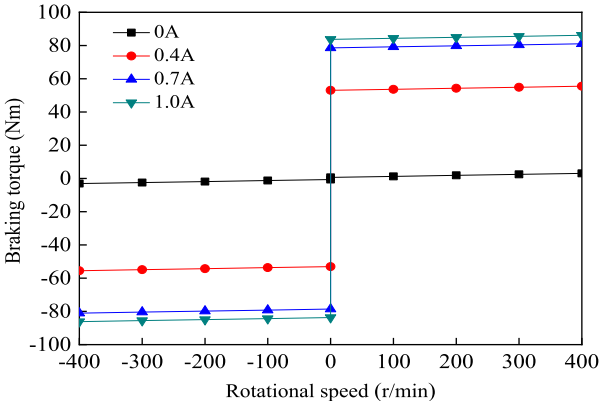

FIGURE 12. Variation of the optimized braking torque with rotational speed.

different speeds can be used as braking torque under a certain current.

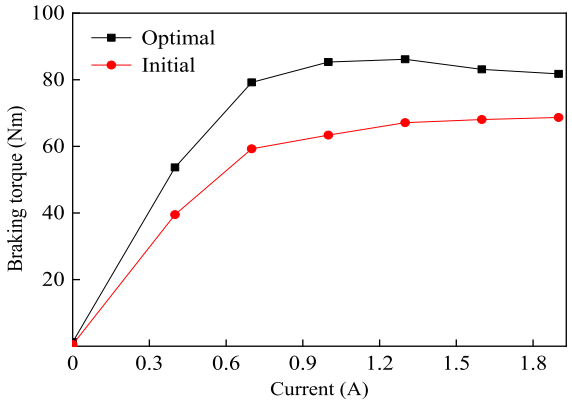

FIGURE 13. Simulation result of braking torque of MR brake.

FIGURE 13 shows the simulated braking torque of the initial and optimal MR brake with the current. It can be seen that the torque of the optimal MR brake is 85.33 N·m at the current of 1 A, which is 34.6% higher than the 63.39 N·m of initial MR brake. In addition, the optimal braking torque shows a downward trend after the applied exceeds 1.4 A. The reason is that MR fluid can reach about 71 kPa saturated shear yield stress at a magnetic flux density of 0.53 T, once the average magnetic flux density in the effective area increases above 0.53 T, the shear yield stress will not continue to be improved. According to equation (31), the calculated shear yield stress has an inflection point when the magnetic flux density is greater than 0.53 T.

V. EXPERIMENTAL ANALYSIS OF THE PROPOSED MR BRAKE

A. PROTOTYPE OF MR BRAKE AND PERFORMANCE TEST SYSTEM

According to the basic structure of the MR brake and the structural size parameters in TABLE 3, the prototypes of initial design and optimal design of the rotary MR brake

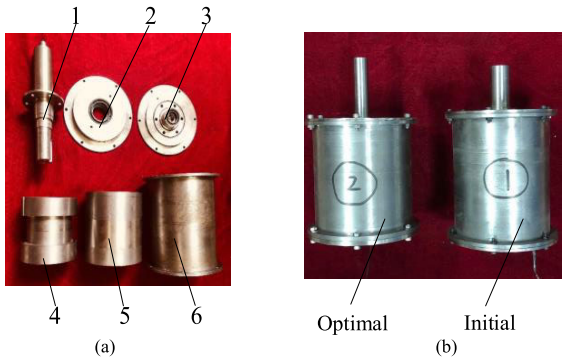

FIGURE 14. Prototypes of the proposed MR brake: (a) Components, and (b) Prototypes. (1) Rotating shaft (2) Left end cover (3) Right end cover (4) Magnetic core (5) Rotating sleeve (6) Cylinder tube.

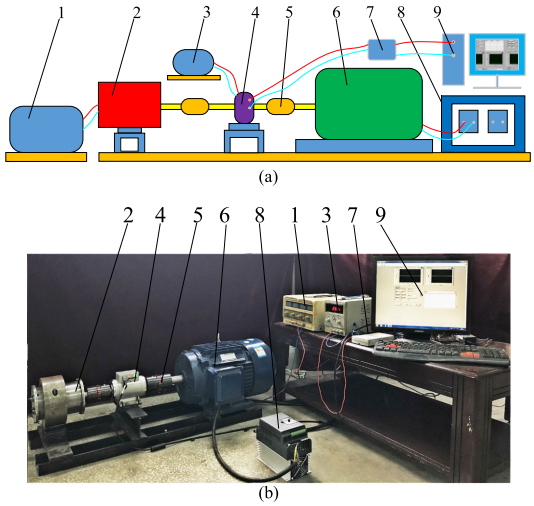

FIGURE 15. Experimental test rig: (a) Schematic diagram of test system, and (b) Test rig. (1) DC Power I (2) MR brake (3) DC Power II (4) Rotational speed and torque sensor (5) Coupling (6) Three-phase AC motor (7) Capture card (8) Frequency converter (9) Computer.

are manufactured, which are shown in FIGURE 14. Among them, the optimized brake prototype is fabricated with the size obtained by the weight coefficient of $\lambda_1 = 0.7$ and $\lambda_2 = 0.3$.

Experimental test rig for dynamic performance of MR brake is shown in FIGURE 15. The test rig consists of a motor drive system and LabVIEW data acquisition system. The MR brake is connected with rotational speed and torque sensor through the coupling and driven by three-phase AC motor after speed regulation. The NI-USB-6210 multi-function capture card is used to obtain the speed and torque voltage signals of the sensor, then the voltage signal is filtered by the LabVIEW data acquisition software in the computer, and the accurate speed and torque of the multiple fluid flow channels are obtained after calculation. A DC Power I was used to supply power to the excitation coil in the MR brake, and the DC Power II is used to supply power to the rotational speed and torque sensor.

B. COMPARISON OF TORQUE PERFORMANCE OF INITIAL AND OPTIMAL BRAKES

FIGURE 16 shows the braking torque under different rotational speeds for the initial and optimal MR brake. It can be concluded that braking torques of initial MR brake and optimal MR brake increase as the increase of the applied current, and the growth trend gradually decline when the current is relatively large. The variation trends of initial and optimal MR brake are basically the same. However, the growth trend becomes slower obviously after the current exceeds 1.2 A for the initial MR brake, and the optimal MR brake still has a large increase in the range of 1.2-1.6 A. The results manifest that the optimal braking torque tends to saturation state when the current reaches 1.8 A. When the speed is 200 r/min, the maximum braking torque of the optimal MR brake can reach 65.69 N·m. Compared with the 58.05 N·m of the initial one, the torque performance is improved by 13.2%.

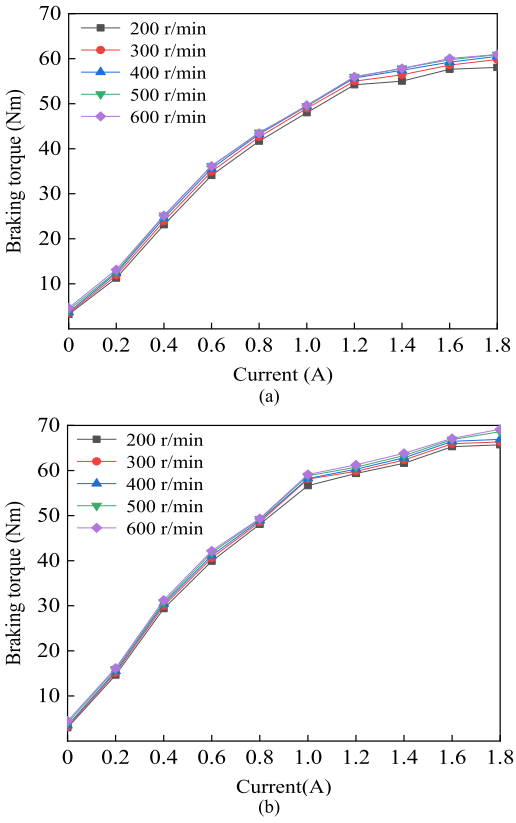

FIGURE 16. Experimental braking torque with current under different rotational speed: (a) Initial MR brake, and (b) Optimal MR brake.

FIGURE 17 shows the braking torque of the initial and optimal MR brake at the rotational speed of 600 r/min. Since the distribution of magnetic flux lines in the damping gap of the optimal MR brake is more concentrated and uniform, the magnetic flux density is larger than that initial one under the same current, and the magnetic flux density increased faster with the current, which is consistent with the results

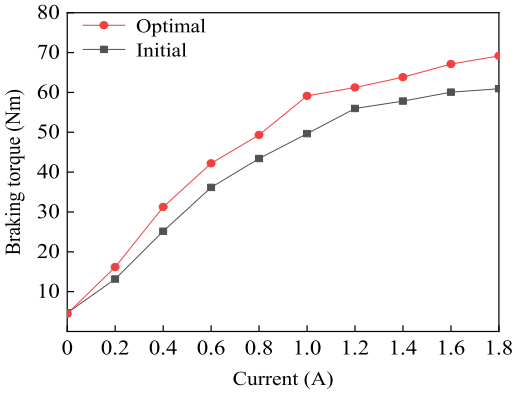

FIGURE 17. Experimental braking torque with current under fixed rotational speed.

obtained by simulation analysis. When the applied current is 1.8 A, the maximum braking torque of the optimal MR brake can reach 69.16 N·m. Compared with the initial one of 60.92 N·m, the torque performance is improved by 13.5%.

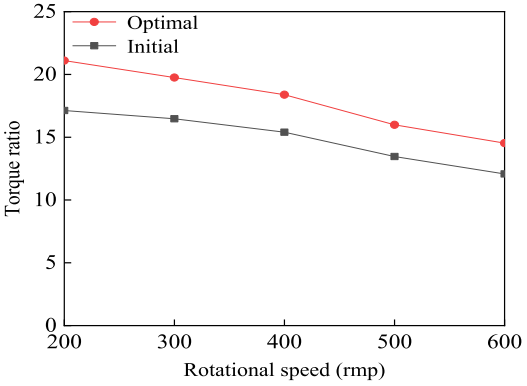

FIGURE 18. Experimental torque ratio with rotational speed.

FIGURE 18 shows torque ratio of the initial and optimal MR brakes varying with the rotational speed. It can be seen that the torque ratio of the optimal MR brake increases significantly compared to the initial one. When the rotational speed is 200 r/min, the torque ratio of the optimal MR brake is 21.1, which is 2.3% higher than the initial one of 17.12. In addition, the torque ratio of the initial and optimal brakes all decrease with the increase of rotational speed, which is mainly because the viscous induced torque increases at a higher rate than the magnetic induced torque.

C. COMPARISON OF SIMULATED AND EXPERIMENTAL TORQUE PERFORMANCE

FIGURE 19 shows the comparison curve between the experimental and the simulated braking torque of the initial and optimal MR brake at the rotational speed of 300 r/min. When the applied current is small, the experimental braking torques of initial and optimal MR brake are slightly larger than that simulated braking torque, mainly because the friction torque

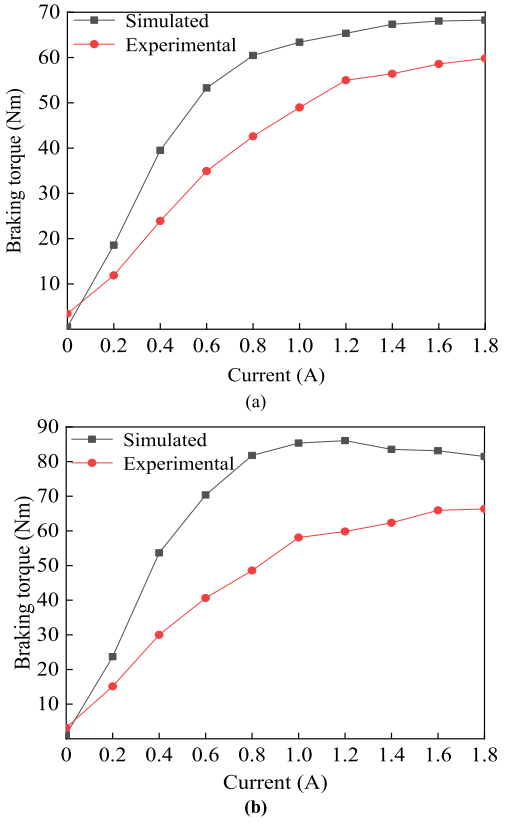

FIGURE 19. Comparison between simulated and experimental braking torque: (a) Initial MR brake, and (b) Optimal MR brake.

of the MR brake itself is included in the braking torque. With the increase of the applied current, the simulated braking torque begins to exceed the experimental braking torque, because the magnetic induced braking torque accounts for the main part of the total braking torque.

In the magnetic field simulation analysis, the ideal boundary conditions are used to ignore the magnetic leakage phenomenon, which leads to a certain difference between the experimental value and the simulation result. In addition, when using the Bingham model to derive the mathematical model of braking torque, the shear thinning phenomenon of MR fluid and temperature effect on the actual torque is not considered.

D. ANALYSIS OF BRAKING TORQUE PERFORMANCE

FIGURE 20 shows the braking torque change of the initial and optimal MR brakes under different rotational speeds and applied currents. It can be concluded from FIGURE 20 that, at the same current, the braking torque increases slightly with the increase of rotational speed. According to equation (30), due to the characteristic that the viscous induced torque increases with the rotational speed, the brake viscous induced torque does not contribute much to the total braking torque of the MR brake. Thus, the change of rotational speed has little impact on the braking torque under a fixed current. Especially at low and medium rotational speeds. The rotational speed

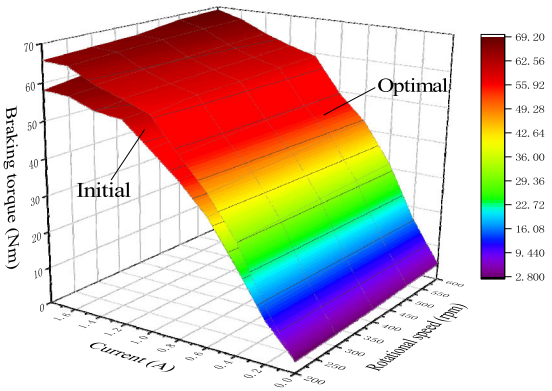

FIGURE 20. Dynamic variation of braking torque of initial and optimal MR brakes under different currents and rotational speed.

is approximately independent of the braking characteristics, which has important practicability for reducing the design difficulty of MR brake control strategy. At the same time, the characteristic that braking torque does not change with the rotational speed, can make MR brake is applied for braking function in high-speed running occasions, and can also be applied as a deceleration buffer mechanism.

Observing FIGURE 20, It can be seen that the optimal braking torque increases from the initial value of about 3.5 N·m to about 69.16 N·m with the current change. When the current is 0.6-1.2 A, the distance between different torque curves with the same current variation is basically the same, which indicates that the MR brake has good control characteristics in this current range. When the current is 1.2-1.8 A, the distance between adjacent torque curves decreases significantly, indicating that the magnetic field intensity tends to saturation state.

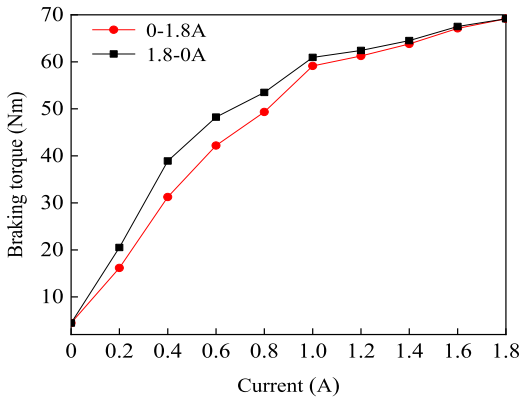

FIGURE 21. Hysteresis characteristic of braking torque.

Two different current variation modes of loading and unloading are adopted. Firstly, the current is linearly loaded from 0 A to 1.8A, and then it decreases linearly from 1.8 A to 0 A. The current interval of the two current variation modes is 0.2 A. FIGURE 21 shows the hysteresis curve of the MR brake when the rotation speed is 600 r/min. It can be seen that braking torque during unloading is greater than that during loading with the same speed and current. The misalignment of torque curve is due to the hysteresis characteristic of brake magnetic circuit material during the current unloading process. And the larger the vertical distance between the two curves, the greater the hysteresis loss of the material will be, which in turn brings greater heat and energy loss. Under two different current loading modes, the optimal MR brake has a smaller braking torque difference at the same current and has a promising hysteresis characteristic.

VI. CONCLUSION

In this paper, a rotary MR brake with multiple fluid flow channels was proposed and designed. By inserting the non-magnetic ring in the middle of the magnetic conduction sleeves, the magnetic flux can be guided to the external fluid flow channel, and the effective damping gaps are increased from two sections to four sections, so the torque performance can be greatly improved under a constrained volume.

With the radial dimension and damping gap size of the MR brake unchanged, the first-order optimization algorithm of ANSYS was adopted to perform multi-objective optimization on the braking torque and torque ratio. The simulation results show that the braking torque and torque ratio increase from 63.39 N·m and 33.33 of initial design to 85.33 N·m and 34.38 of optimal design, respectively.

When the current is 1.8 A and the rotational speed is 600 r/min, the experimental results show that the maximum braking torque of the optimal MR brake can reach 69.16 N·m, which is 13.5% higher than the initial brake. When the current is 1.8 A and rotational speed is 200 r/min, the maximum torque ratio of optimal design is 21.1, which is 2.3% higher than the initial design. The brake torque is basically not affected by the change of speed at the same current. Meanwhile, the variation trends of the experimental results are mainly the same as the simulation results, indicating that the proposed MR brake meets the expected requirements, and the effectiveness of the optimal design is also verified.

REFERENCES

[1] J. S. Kumar, P. S. Paul, G. Raghunathan, and D. G. Alex, "A review of challenges and solutions in the preparation and use of magnetorheological fluids," *Int. J. Mech. Mater. Eng.*, vol. 14, no. 1, pp. 1–18, Dec. 2019.
[2] Y. Zhang, D. Li, H. Cui, and J. Yang, "A new modified model for the rheological properties of magnetorheological fluids based on different magnetic field," *J. Magn. Magn. Mater.*, vol. 500, Apr. 2020, Art. no. 166377.
[3] N. Faraz, H. Lei, and Y. Khan, "Analytical solution of linear, quadratic and cubic model of PTT fluid," *J. Appl. Comput. Mech.*, vol. 1, no. 4, pp. 220–228, 2015.
[4] M. N. Aruna, M. R. Rahman, S. Joladarashi, and H. Kumar, "Investigation of sedimentation, rheological, and damping force characteristics of carbonyl iron magnetorheological fluid with/without additives," *J. Brazilian Soc. Mech. Sci. Eng.*, vol. 42, pp. 228–241, 2019.
[5] T. Potisk, D. Svenšek, H. Pleiner, and H. R. Brand, "Continuum model of magnetic field induced viscoelasticity in magnetorheological fluids," *J. Chem. Phys.*, vol. 150, no. 17, May 2019, Art. no. 174901.
[6] G. Hu, L. Li, H. Liu, and F. Liu, "Effects of winding cylinder materials on dynamic performances of a new MR damper," *IEEE Access*, vol. 8, pp. 87829–87841, 2020.
[7] G. Hu, H. Liu, J. Duan, and L. Yu, "Damping performance analysis of magnetorheological damper with serial-type flow channels," *Adv. Mech. Eng.*, vol. 11, no. 1, pp. 1–12, Nov. 2019.

[8] G. Hu, F. Yi, W. Tong, and L. Yu, "Development and evaluation of a MR damper with enhanced effective gap lengths," *IEEE Access*, vol. 8, pp. 156347–156361, 2020.
[9] S. S. Sun, D. H. Ning, J. Yang, H. Du, S. W. Zhang, W. H. Li, and M. Nakano, "Development of an MR seat suspension with self-powered generation capability," *Smart Mater. Struct.*, vol. 26, no. 8, Aug. 2017, Art. no. 085025.
[10] G. Hu, J. Zhang, F. Zhong, and L. Yu, "Performance evaluation of an improved radial magnetorheological valve and its application in the valve controlled cylinder system," *Smart Mater. Struct.*, vol. 28, no. 4, Apr. 2019, Art. no. 047003.
[11] G. Hu, M. Liao, and W. Li, "Analysis of a compact annular-radial-orifice flow magnetorheological valve and evaluation of its performance," *J. Intell. Mater. Syst. Struct.*, vol. 28, no. 10, pp. 1322–1333, Jun. 2017.
[12] E. M. Binyet and J. Chang, "Magnetohydrodynamics modelling of a permanent magnets activated MRF clutch–brake," *Microsyst. Technol.*, Jun. 2020, doi: 10.1007/s00542-020-04910-w.
[13] H. Qin, A. Song, and Y. Mo, "Performance evaluation of a hollowed multi-drum magnetorheological brake based on finite element analysis considering hollow casing radius," *IEEE Access*, vol. 7, pp. 96070–96078, 2019.
[14] S. Li, W. Meng, and Y. Wang, "Numerical and experimental studies on a novel magneto-rheological fluid brake based on fluid–solid coupling," *Sci. Prog.*, vol. 103, no. 1, pp. 1–33, 2020.
[15] Q. H. Nguyen and S. B. Choi, "Optimal design of a novel hybrid MR brake for motorcycles considering axial and radial magnetic flux," *Smart Mater. Struct.*, vol. 21, no. 5, May 2012, Art. no. 055003.
[16] S. R. Patil, K. P. Powar, and S. M. Sawant, "Thermal analysis of magnetorheological brake for automotive application," *Appl. Thermal Eng.*, vol. 98, pp. 238–245, Apr. 2016.
[17] J. Huang, J. Q. Zhang, Y. Yang, and Y. Q. Wei, "Analysis and design of a cylindrical magneto-rheological fluid brake," *J. Mater. Process. Technol.*, vol. 129, nos. 1–3, pp. 559–562, Oct. 2002.
[18] J. Wu, X. Jiang, Q. Li, J. Yao, H. Li, and Z. Li, "Design and modelling of a novel multilayered cylindrical magnetorheological brake," *Int. J. Appl. Electromagn. Mech.*, vol. 53, no. 1, pp. 29–55, 2017.
[19] K. Karakoc, E. J. Park, and A. Suleman, "Design considerations for an automotive magnetorheological brake," *Mechatronics*, vol. 18, no. 8, pp. 434–447, Oct. 2008.
[20] T. Kikuchi and K. Kobayashi, "Design and development of cylindrical MR fluid brake with multi-coil structure," *J. Syst. Des. Dyn.*, vol. 5, no. 7, pp. 1471–1484, 2011.
[21] T. Nam and K. Ahn, "A new structure of a magnetorheological brake with the waveform boundary of a rotary disk," *Smart Mater. Struct.*, vol. 18, no. 11, 2009, Art. no. 115029.
[22] D. Senkal and H. Gurocak, "Compact MR-brake with serpentine flux path for haptics applications," in *Proc. World Haptics-3rd Joint Euro-Haptics Conf. Symp. Haptic Interfaces Virtual Environ. Teleoperator Syst.*, Mar. 2009, pp. 91–96.
[23] H. Qin, A. Song, and Y. Mo, "A hybrid actuator with hollowed multi-drum magnetorheological brake and direct-current micromotor for hysteresis compensation," *J. Intell. Mater. Syst. Struct.*, vol. 30, no. 1, pp. 1–12, 2019.
[24] Y. Shiao and Q.-A. Nguyen, "Development of a multi-pole magnetorheological brake," *Smart Mater. Struct.*, vol. 22, no. 6, Jun. 2013, Art. no. 065008.
[25] H. Wang and C. Bi, "Study of a magnetorheological brake under compression-shear mode," *Smart Mater. Struct.*, vol. 29, no. 1, Jan. 2020, Art. no. 017001.
[26] B. Assadsangabi, F. Daneshmand, N. Vahdati, M. Eghtesad, and Y. Bazargan-Lari, "Optimization and design of disk-type MR brakes," *Int. J. Automot. Technol.*, vol. 12, no. 6, pp. 921–932, Dec. 2011.
[27] Q. H. Nguyen and S. B. Choi, "Optimal design of an automotive magnetorheological brake considering geometric dimensions and zero-field friction heat," *Smart Mater. Struct.*, vol. 19, no. 11, Nov. 2010, Art. no. 115024.
[28] Q. Nguyen and S. B. Choi, "Selection of magnetorheological brake types via optimal design considering maximum torque and constrained volume," *Smart Mater. Struct.*, vol. 21, no. 1, 2012, Art. no. 015012.
[29] H. Qin, A. Song, and Y. Mo, "Evaluation of a multi-drum magnetorheological brake via finite element analysis considering number of drums and fluid gap selection in optimization," *J. Intell. Mater. Syst. Struct.*, vol. 30, no. 5, pp. 778–787, Mar. 2019.
[30] T. Le-Duc, V. Ho-Huu, and H. Nguyen-Quoc, "Multi-objective optimal design of magnetorheological brakes for motorcycling application considering thermal effect in working process," *Smart Mater. Struct.*, vol. 27, no. 7, Jun. 2018, Art. no. 075060.
[31] S. Mousavi and H. Sayyaadi, "Optimization and testing of a new prototype hybrid MR brake with arc form surface as a prosthetic knee," *IEEE/ASME Trans. Mechatronics*, vol. 23, no. 3, pp. 1204–1214, Jun. 2018.
[32] O. Topcu, Y. Taçcioğlu, E. İ. Konukseven, "Design and multi-physics optimization of rotary MRF brakes," *Results Phys.*, vol. 8, pp. 805–818, Mar. 2018.

GUOLIANG HU received the Ph.D. degree from Zhejiang University, China, in 2006. He is currently a Professor with East China Jiaotong University, where he is also the Director of the Key Laboratory of Conveyance and Equipment, Ministry of Education. He is involved in the projects sponsored by the National Natural Science Foundation of China and by the Natural Science Foundation of Jiangxi Province. He has published more than 180 technical articles in refereed international journals and conferences. His research interests include smart materials and structures and fluid power transmission and control.

LIFAN WU is currently pursuing the M.S. degree with the School of Mechatronics and Vehicle Engineering, East China Jiaotong University. His research interest includes design and analysis of rotary magnetorheological brake with multiple fluid flow channels.

LINSEN LI received the B.Sc. and M.Sc. degrees in mechanical engineering from East China Jiaotong University, in 2016 and 2020, respectively. His research interests include design and performance analysis of magnetorheological brake and damper.

LIFAN YU received the B.Sc. and M.Sc. degrees in mechanical engineering from East China Jiaotong University, in 2011 and 2014, respectively. He is currently a Laboratory Staff with the School of Mechatronics and Vehicle Engineering, East China Jiaotong University. His research interests include design, simulation, and experimental verifications of new magnetorheological valve and damper.